Research Article

Jian Zhang, Dandan Wang, Yunbin Ying, Hao Zhou, Xiaokai Liu, Xin Hu, Yingxin Chen, Qiang Li*, Xuefeng Zhang* and Min Qiu*

Grayscale-patterned metal-hydrogel-metal microscavity for dynamic multi-color display

https://doi.org/10.1515/nanoph-2021-0413
Received July 28, 2021; accepted September 20, 2021; published online October 11, 2021

Abstract: Dynamic structural color based on tunable optical resonance plays a key role in applications including encryption visualization, camouflage and colorimetric sensing. However, the current design requires either complex growth processes of the high-quality tunable materials or complicated circuit designs. This work makes a humidity-swelling hydrogel layer for metal–insulator–metal (MIM) structure in the dynamic multi-color display. Here, polyvinyl alcohol (PVA) hydrogel structure is patterned through grayscale e-beam lithography and the controlled PVA thickness leads the programmable reflective resonance covering the entire visible range. By varying the ambient humidity between 9.8 and 90.1% RH, the reflective resonance of the structure is tailored across a wavelength range over 100 nm. Our materials platform of humidity-sensitive hydrogel resist presents a novel approach of the stepwise and reversible optical tunability for photonic devices.

Jian Zhang, Dandan Wang, and **Yunbin Ying** contributed equally.

***Corresponding authors: Qiang Li**, State Key Laboratory of Modern Optical Instrumentation, College of Optical Science and Engineering, Zhejiang University, Hangzhou 310027, P. R. China, E-mail: qiangli@zju.edu.cn; **Xuefeng Zhang**, College of Materials and Environmental Engineering, Institute of Advanced Magnetic Materials, Hangzhou Dianzi University, Hangzhou, 310018, P. R. China, E-mail: zhang@hdu.edu.cn; and **Min Qiu**, Key Laboratory of 3D Micro/Nano Fabrication and Characterization of Zhejiang Province, School of Engineering, Westlake University, Hangzhou 310024, P. R. China, E-mail: qiu_lab@westlake.edu.cn

Jian Zhang, Dandan Wang, Hao Zhou, Xiaokai Liu, Xin Hu and Yingxin Chen, College of Materials and Environmental Engineering, Institute of Advanced Magnetic Materials, Hangzhou Dianzi University, Hangzhou, 310018, P. R. China. https://orcid.org/0000-0001-7181-6021 (J. Zhang)

Yunbin Ying, State Key Laboratory of Modern Optical Instrumentation, College of Optical Science and Engineering, Zhejiang University, Hangzhou 310027, P. R. China

Keywords: dynamic structural color; grayscale exposure; hydrogel microstructure; multi-color display.

1 Introduction

Structural color generated from subwavelength structural designs are advantageous over conventional chemical colors because of their resistance to high temperature and irradiation exposure [1–3]. For structural color, the color rendering is sensitively related to geometric deformation, surrounding media and component change, thus offering a new degree of freedom for dynamic color control [4–6]. Existing materials systems of structural colors, however, has fixed color upon fabrication and cannot be used for dynamic multi-color display. Active materials allowing real-time changes of its optical properties is under exploration for applications including encryption visualization, camouflage and colorimetric sensing [7–9].

MIM multi-layer structures allow high-efficient bandpass filtering by the multi-layer interference [10–13]. With the ultrathin lossy metallic layer on top, the constructive and destructive interference are formed in MIM structures due to the control of optical phase within the transparent insulator layer. The interference resonance is impacted with the thickness and the effective reflective index of the insulator layer. Thus, this construction enables dynamic multi-color displays using a tunable insulator layer based on electro/chemical-active or temperature-sensitive materials [7, 14–16]. For example, electrochromic materials, such as tungsten oxide and iron oxide, are induced in the insulator layer and the migration of ions during charge/discharge states resulting in the vibration of reflective index and the color change [17, 18]. To allow external electric fields for tuning, complicated capacitor designs are required. Phase-change materials (chalcogenides [19–21], vanadium oxide [22, 23], et al.) are also widely reported for real-time tunable plasmonic resonance, but growth processes of high-quality layers are demanding. With controlled hydrogenation and dehydrogenation processes, metal hydrides (MgH_2, TiH_2, et al.) can be reversed between

metal and dielectric and thus the optical properties can be switched [24, 25]. This method requires a safe control of hydrogen input, which is unexpected for common usage in dynamic display.

Hydrogel films own the self-driven swelling/shrinking behavior by the change of environmental humidity and can be prepared by spin-coated conveniently [26]. Compared with the current approaches, hydrogel film is in perspective for tunable structural color with the advantages of ease access, fast responsibility and nearly lossless in visible range [27–30]. For MIM structures, the combination of hydrogel films as the insulator layer allows the swellable thickness leading to the adjustable multi-layer interference by humidity control [31, 32]. Various patterning techniques (e.g. laser printing [33], mask-aligned light exposure [32, 34], and 2D/3D printing method [27, 35, 36]) are developed for hydrogel-based structural color, and are mainly limited in macroscale. Aiming the application in photonic devices, a multi-color programmable and high-resolution patterning method is still desired, and are challenging due to the structural collapse and deformation of hydrogel materials.

It is proved that electron beam lithography, as one of the ultrahigh-resolution patterning techniques [37], can irradiate hydrogel chains within nanospots and form designable micro-/nanostructures [38, 39]. In this work, we propose the MIM structure by inducing hydrogel as the active insulator layer of which the thickness is tunable by humidity change. As the e-beam lithographic (EBL) resist, polyvinyl alcohol (PVA) is competent for grayscale exposure, and the insulator thickness and the reflective resonance is accurately programmed by exposure dose. Combined with a thick aluminum (Al) layer at the bottom and a thin platinum (Pt) layer at the top, asymmetric Fabry–Perot cavity is formed and preforms multi-color display covering the visible range. Furthermore, the hydrogel structures after e-beam exposure still perform quick swelling/shrinking response to humidity change, and promises a novel approach of the stepwise and reversible optical tunability.

2 Results and discussion

The color generation of the MIM structure directly depends on the thickness of the insulator layer, as the schematic configuration shown in Figure 1(a). An Al bottom layer is deposited with the thickness (H_{Al}) over 200 nm for entire reflection in visible wavelength range [40], and PVA is patterned as the insulator layer followed by coating a thin Pt layer with the thickness (H_{Pt}) of 27 nm on top (as the SEM image shown in the inset of Figure 1(a)). To pattern the negative-tone PVA resist, EBL is carried out with a low acceleration voltage of 5 kV, which can efficiently reduce

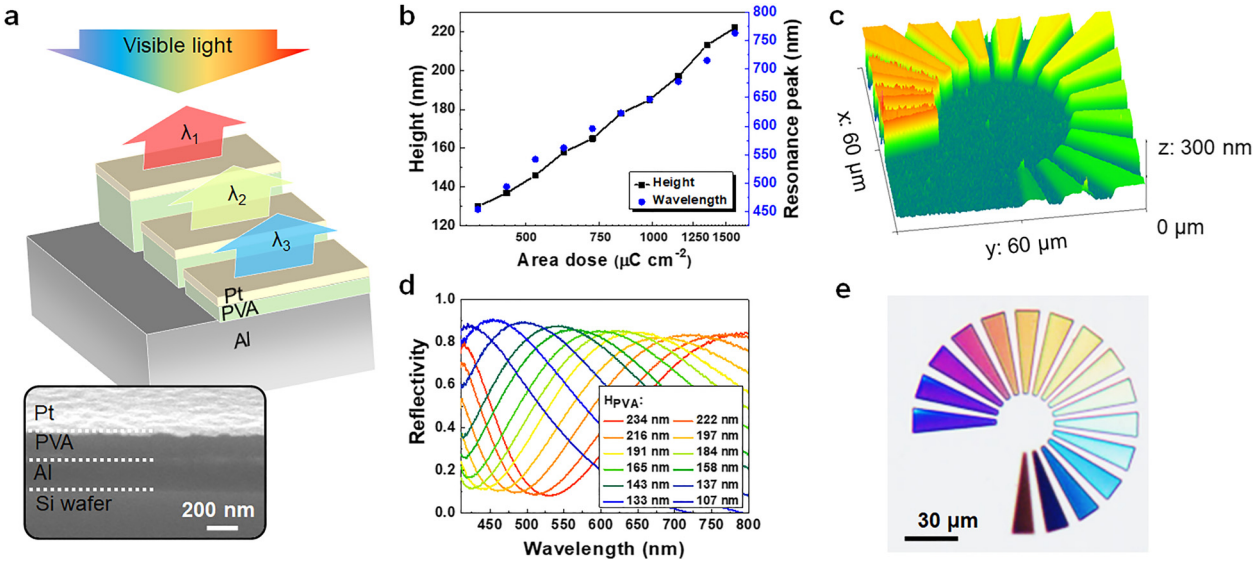

Figure 1: (a) Schematics of the proposed MIM microstructure with the varied insulator thickness for multi-color displays. Inset shows the cross-section SEM image of Pt/PVA/Al (thickness: 27 nm/140 nm/150 nm, respectively) layers on a Si wafer. (b) Height of exposed PVA and reflective resonance of the corresponding MIM structures with varied EBL exposure dose. (c) Height map tested by AFM for patterned MIM structure. (d) Reflection spectra of MIM structure containing the PVA layer with the thickness varied from 107 to 224 nm, and the top Pt layer with the thickness of 14 nm. (e) Photograph of the patterned MIM structure showing multi-color display with increased thickness from 107 to 224 nm.

the sensitivity of the PVA resist and the exposure time [41, 42]. The contrast value (γ) of the PVA resist is calculated as 0.91 (described in Figure S1), which is lower than the reported polystyrene and SU-8 resist ($\gamma \sim 1.0$) [41, 43], proving the competent capability for grayscale exposure. Based on this contrast test, Figure 1(b) proves that with varied exposure dose between 300 and 1500 μC cm^{-2}, the PVA thickness (H_{PVA}) is gradually controlled between 107 and 234 nm. The height image measured with AFM in Figure 1(c) shows the final result of grayscale-exposed patterns. Corresponding to the increased PVA thickness, the reflective resonance of MIM structure is tuned between the wavelength of 450 and 780 nm in Figure 1(d), and the color change is shown in the inset of Figure 1(e). The relationship between the PVA thickness and reflective resonance is concluded in Figure 1(b).

The top thin layer plays an important role for the strong cavity confinement, and its impact on reflection is investigated by varying thickness. Figure 2(a) represents the patterns deposited with H_{Pt} of 0, 5, 14, 27, and 36 nm, respectively. It can be seen that by increasing the Pt thickness over 14 nm the multi-color display of the palettes is obvious. Furthermore, Figure 2(b) and (c) shows the impacts from varied Pt thickness on reflection spectra with the initial PVA thickness of 137 and 216 nm, respectively. It is clearly shown that by increasing the Pt thickness from zero to 36 nm, the reflective resonance is blue-shifted and the reflective intensity is gradually enhanced. The thicker Pt layer enhances the reflection from the Pt–air interface and increase the reflective intensity. Also, the accumulated phase shift is varied with the thickness of Pt layer, making the resonance blue shifted [29, 44]. The detailed reflection spectra of the PVA layers with the thickness varied from 107 to 234 nm and coated with 14 and 27 nm are concluded in Figure 1(d) and S2, proving the structural color covering the entire visible range. Based on this, the color gamut of our grayscale exposed patterns on CIE 1931 Chromaticity Diagram is calculated and represented in Figure 2(d), demonstrating a broad coverage in sRBG color space for multi-color display.

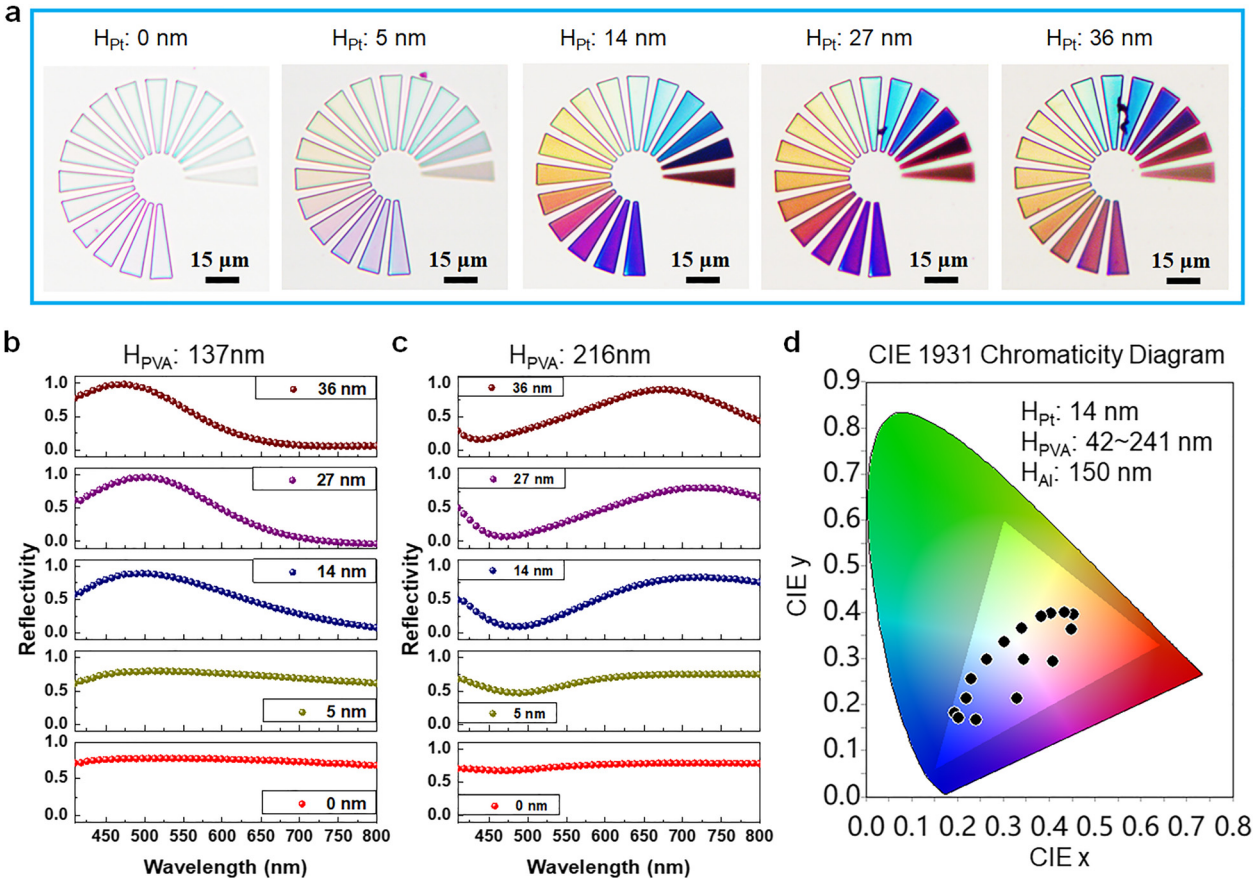

Figure 2: (a) Photograph of multi-color palettes coated with H_{Pt} of 0, 5, 14, 27, 36 nm, respectively. Reflection spectra of PVA layers with H_{PVA} of (b) 137 and (c) 216 nm, coated with H_{Pt} of 0, 5, 14, 27, 36 nm, respectively. (d) CIE 1931 color coordinate variation diagram based on Fabry–Perot cavities with varied H_{PVA} between 107 and 234 nm, and H_{Pt} of 14 nm.

The main limiting factor of humidity tunability for this hydrogel-based Fabry–Perot cavities is the impedance from the coverage of the top Pt layer, which may impact the swelling ability of the hydrogel layer. As shown in Figure S3, the color change is not uniform for Pt layer with 36 nm thickness. To avoid this problem, grayscale-patterned PVA structures coated with 14 nm-thick Pt is mainly utilized for the further study of humidity-tunable structural color.

The reflective mechanism of MIM multi-layer structures is well discussed as asymmetric Fabry–Perot cavity in the previous reports [45–47]. Assuming the PVA layer is semi-infinite and the top Pt layer is ultra-thin (illustrated in Figure 3(a)), the reflection and transmission coefficients for the wave propagating from air to PVA layer, from PVA layer to air, and from PVA layer to Al layer are r_a and t_a, r_b and t_b, r_s and t_s, respectively. Based on the Fresnel reflection theory, the multi-layer interference in Fabry–Perot cavity leads the reflection coefficient r and the phase accumulation β through the insulator layer as:

$$r = r_a + \left(t_a t_b r_s e^{i2\beta}\right) \Big/ \left(1 - r_b r_s e^{i2\beta}\right) \quad (1)$$

$$\beta = 2\pi n_{PVA} h_{PVA} \cos(\theta_c)/\lambda \quad (2)$$

where n_{PVA}, h_{PVA}, θ_c and λ are the refractive index of PVA, the thickness of PVA layer, the refraction angle and the wavelength. And the reflectivity R can be calculated as $R = |r|^2$. In Eq. (1), the increasing thickness of the top Pt layer leads to the greater r_a and thus enhances the total reflective intensity, as proved in Figure 2(b) and (c). The detailed reflection spectra are simulated to examine the thickness effect of hydrogel layer on the resonance. Figure 3(b) and (c) compare the measured and calculated reflectance spectra for the structures with varied hydrogel thickness (H_{PVA} = 133, 184, 222 nm), of which the reflective resonances matching well with each other for normal incidence. The simulated electric field distributions of the vertical cross-section of the MIM structures in Figure 3(d) and (f) prove that there is a typical Fabry–Perot dominated resonance existing in the hydrogel layer at all of the reflective resonances at 448, 623, 753 nm for the hydrogel thickness of 133, 184, 222 nm, respectively.

It is proved by our previous work that the hydrophilic groups of PVA after e-beam exposure are still kept, and the swelling/deswelling responsibility to humidity change is retained [38]. To elucidate the resonance tunability of our hydrogel-based Fabry–Perot cavities, the reflection spectra are recorded by varying ambient humidity from 9~90% RH in Figure 4(a)–(c). The reflective colors of the structure with the initial PVA thickness of 133, 185, 216 nm are blue, yellow and red, respectively. By increasing the ambient

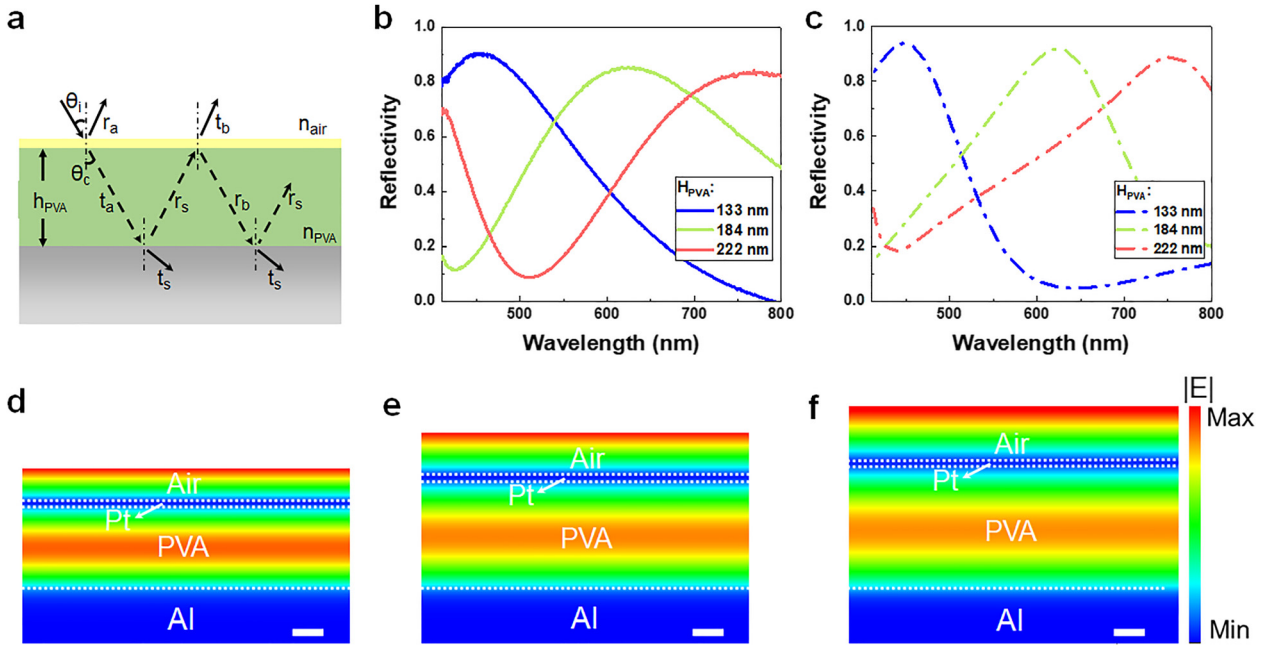

Figure 3: (a) Schematic of the multi-layer interference, in which the reflection and transmission coefficients within multi-layers are illustrated. (b) Measured reflection spectra of the structure with H_{Pt} = 14 nm, and H_{PVA} = 133, 184, 222 nm, respectively. (c) Simulated reflection spectra of the structure with H_{Pt} = 14 nm, and H_{PVA} = 133, 184, 222 nm, respectively. Electric field distributions of the vertical cross-section of the structure at the reflective resonances of (d) 448, (e) 623, (f) 753 nm with the hydrogel thicknesses of 133, 184, 222 nm, respectively. The scale bar in (d)–(f) is 50 nm.

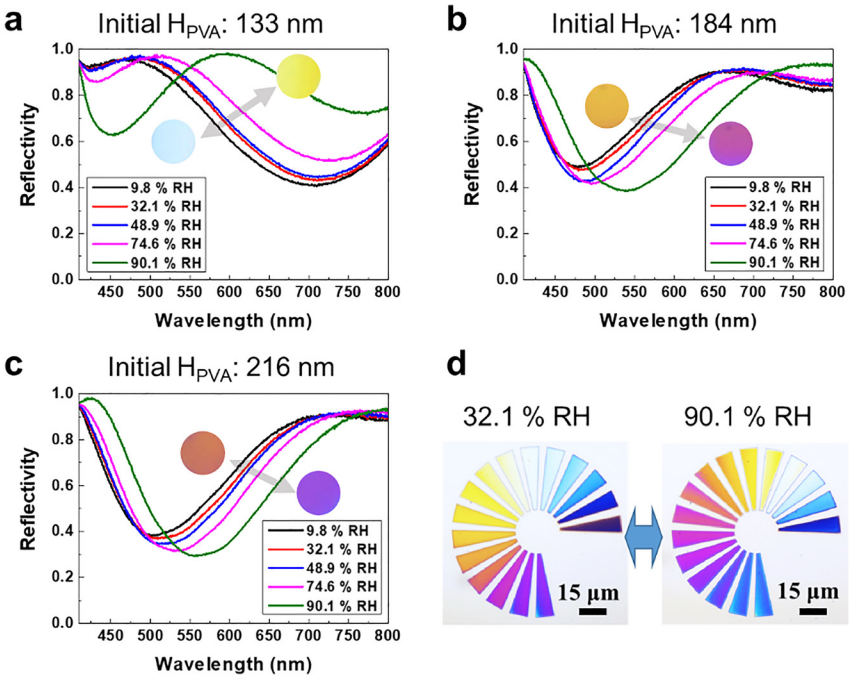

Figure 4: Refection spectra of the structures with the initial H_{PVA} of (a) 133 nm, (b) 184 nm, (c) 216 nm, and H_{Pt} of 14 nm. Inset shows the actual colors at 32.1 and 90.1% RH. (d) Photograph of multi-color palettes switched with ambient humidity between 32.1 and 90.1% RH.

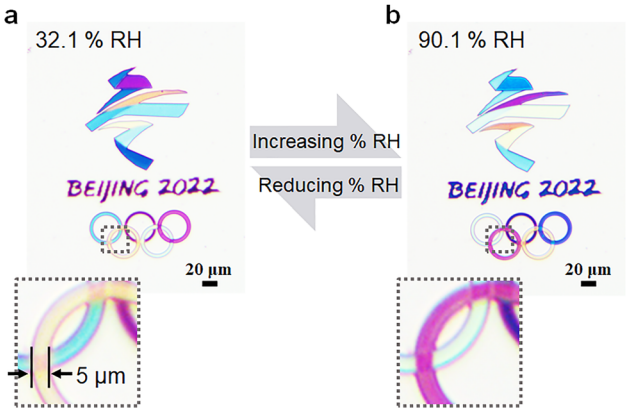

Figure 5: Logo pattern of the Beijing 2022 olympic games which is tunable by switching humidity between 32.1 and 90.1% RH.

humidity from 9.8 to 90.1% RH, all the structures show the stepwise resonance shift and obvious color change due to the film swelling. For intuitionistic expression, the photograph in Figure 3(d) concludes the color change covering the entire visible range between the ambient humidity of 32.1–90.1% RH.

Finally, the resolution and dynamic multi-color printing of hydrogel-based Fabry–Perot cavities is verified in this work. The microscopic images in Figure 5 shows the logo pattern of the Beijing 2022 Olympic Games, which is printed by grayscale exposure of PVA resist. After coating with top Pt layer, the highly-saturated colorful palette is visualized due to the different height of PVA layers. Once exposed to the changed humidity, the color variations can be observed by naked eyes. The line width of the pattern in the zoomed-in area in Figure 5 is 5 μm, and the minimum half-pitch of checkerboard patterns in Figure S4 is realized as 1 μm. This demonstrates the resolution capability and conformal tunability by humidity change. Thus, this proves that our grayscale patterning technique on hydrogel structure is competent for potential applications in dynamic structural color and other optical devices.

3 Conclusions

In summary, we report a novel approach to realize dynamic multi-color display based on hydrogel-based MIM structures. The contrast of PVA resist is as low as 0.91 and is competent for grayscale exposure. By controlling the exposure dose, the PVA structures with accurately-programmable thickness perform strong reflective resonances covering the entire visible range. Furthermore, the hydrogel structures after exposure still keep quick swelling responsibility to humidity change, and perform stepwise and reversible optical tunability. Considering that this deformation capability of hydrogel structure is self-driven and bio-compatible, hydrogel-based plasmonic structures and metastructures could own further applications in complex dynamic nanophotonic devices, such as optical anti-counterfeiting, smart camouflage, and colorimetric sensing.

4 Methods

4.1 Sample fabrication

Wafer substrate is cleaned and coated with 200 nm-thick Al by thermal evaporation. PVA, which can form smooth film by spin-coating and owns high-resolution capability, is utilized as the hydrogel resist. PVA is purchased from Alfa Aesar (molecular distribution between 10,000 and 26,000 g/mol and alcoholysis degree of 87–89%) is dissolved in DI water for spin-coating. By controlling the concentration and spin-coating speed, PVA film with the thickness of 250 nm on Al layer is utilized as the negative EBL resist. The grayscale exposure on PVA resist is carried out by EBL system (Raith Elphy Quantum system) with the acceleration voltage of 5 kV. After exposure, the patterns are developed by DI water for 1 min. The contrast curve is deduced by the height measurement of the PVA patterns with varied exposure dose by atomic force microscope (AFM, JPK NanoWizard 4-NanoScience). The multi-color patterns are realized by controlling the exposure dose between 300 and 1500 μC cm^{-2}, followed by sputtering a thin Pt layer on the top. The fabricated structures are characterized with scanning electron microscope (SEM, Carl Zeiss Sigma 300).

4.2 Optical charaterization

A lab-made flow controlling system is utilized to tune the ambient humidity, by controlling the mixing ratio between the dry N_2 and saturated moisture flows. The mixed flow blows on the sample nearby, and the original reflection intensity (I_s) are recorded by a fiber-based spectrometer (Ocean Optics QE65 Pro) amounted in a microscope (Nikon Digital Camera Head DS-Fi1). Meanwhile, the reflection images are recorded by a CCD camera. And the ambient humidity of the flow is monitored by a humidity sensor (Thorlabs TSP01). The background reflection intensity (I_b) is recorded, and the reflectivity of the samples as a function of wavelength λ is are calculated as $R(\lambda) = I_s/I_b$.

4.3 Simulation

Reflection spectra and near-field profiles are studied using finite-difference time-domain simulation (FDTD solution, Lumerical Inc.). Plane waves with the wavelength range of 200–1000 nm and the electric field E_0 = 1 V/m are utilized for normal incidence. The refractive index of PVA is set to be 1.48. The refractive index of silicon, Al and Pt is obtained in the material library (Palik) [48]. The reflection is collected with a power monitor and the cross-section near-field distributions are collected a profile monitor.

Author contribution: All the authors have accepted responsibility for the entire content of this submitted manuscript and approved submission.

Research funding: The work is supported by the Institute of Advanced Magnetic Materials (Hangzhou Dianzi University) and the Key Laboratory of 3D Micro/Nano Fabrication and Characterization of Zhejiang Province (Westlake University). The authors gratefully acknowledge the Start-up Program of Hangzhou Dianzi University (KYS385618067), the Fundamental Research Funds for the Provincial Universities of Zhejiang (GK219909299001-003), the Zhejiang Provincial Key Research and Development Program (2019C01121), the National Key Scientific Instrument and Equipment Development Project of China (51927802), the National Key Research and Development Program of China (2019YFE0121700), and the National Natural Science Foundation of China (61975181, 61775194).

Conflict of interest statement: The authors declare no competing financial interest.

References

[1] Y. Zhao, Y. Zhao, H. Sheng, et al., "Artificial structural color pixels: a review," *Materials*, vol. 10, no. 8, p. 944, 2017.
[2] A. Kristensen, J. K. W. Yang, S. I. Bozhevolnyi, et al., "Plasmonic colour generation," *Nat. Rev. Mater.*, vol. 2, no. 1, p. 16088, 2016.
[3] Z. Xuan, J. Li, Q. Liu, F. Yi, S. Wang, and W. Lu, "Artificial structural colors and applications," *Innovation*, vol. 2, no. 1, p. 100081, 2021.
[4] A. S. Roberts, A. Pors, O. Albrektsen, and S. I. Bozhevolnyi, "Subwavelength plasmonic color printing protected for ambient use," *Nano Lett.*, vol. 14, no. 2, pp. 783–787, 2014.
[5] Y. Jin, J. Liang, S. Wu, et al., "Electrical dynamic switching of magnetic plasmon resonance based on selective lithium deposition," *Adv. Mater.*, vol. 32, no. 42, p. 2000058, 2020.
[6] Y. Wang, H. Cui, Q. Zhao, and X. Du, "Chameleon-Inspired structural-color actuators," *Matter*, vol. 1, no. 3, pp. 626–638, 2019.
[7] X. Duan, S. Kamin, and N. Liu, "Dynamic plasmonic colour display," *Nat. Commun.*, vol. 8, no. 1, p. 14606, 2017.
[8] Y. Chen, X. Duan, M. Matuschek, et al., "Dynamic color displays using stepwise cavity resonators," *Nano Lett.*, vol. 17, no. 9, pp. 5555–5560, 2017.
[9] S. C. Malek, H.-S. Ee, and R. Agarwal, "Strain multiplexed metasurface holograms on a stretchable substrate," *Nano Lett.*, vol. 17, no. 6, pp. 3641–3645, 2017.
[10] Z. Wang, X. Wang, S. Cong, et al., "Towards full-colour tunability of inorganic electrochromic devices using ultracompact Fabry–Perot nanocavities," *Nat. Commun.*, vol. 11, no. 1, p. 302, 2020.
[11] Z. Yang, Y. Chen, Y. Zhou, et al., "Microscopic interference full-color printing using grayscale-patterned fabry–perot resonance cavities," *Adv. Opt. Mater.*, vol. 5, no. 10, p. 1700029, 2017.
[12] W. Zhang, H. Li, E. Hopmann, and A. Y. Elezzabi, "Nanostructured inorganic electrochromic materials for light applications," *Nanophotonics*, vol. 10, no. 2, pp. 825–850, 2021.
[13] S. Jeon, S.-K. Sung, E.-H. Jang, et al., "Multilayer metal-oxide-metal nanopatterns via nanoimprint and strip-off for multispectral resonance," *Appl. Surf. Sci.*, vol. 428, pp. 280–288, 2018.
[14] S. D. Rezaei, J. Ho, T. Wang, S. Ramakrishna, and J. K. W. Yang, "Direct color printing with an electron beam," *Nano Lett.*, vol. 20, no. 6, pp. 4422–4429, 2020.
[15] H. Kwon and S. Kim, "Chemically tunable, biocompatible, and cost-effective metal–insulator–metal resonators using silk

protein and ultrathin silver films," *ACS Photonics*, vol. 2, no. 12, pp. 1675–1680, 2015.
[16] J. Lv, D. Chen, Y. Du, et al., "Visual detection of thiocyanate based on Fabry–Perot etalons with a responsive polymer brush as the transducer," *ACS Sens.*, vol. 5, no. 2, pp. 303–307, 2020.
[17] J. Chen, Z. Wang, Z. Chen, S. Cong, and Z. Zhao, "Fabry–Perot cavity-type electrochromic supercapacitors with exceptionally versatile color tunability," *Nano Lett.*, vol. 20, no. 3, pp. 1915–1922, 2020.
[18] Z. Yan, Z. Zhang, W. Wu, et al., "Floating solid-state thin films with dynamic structural colour," *Nat. Nanotechnol.*, vol. 16, no. 7, pp. 795–801, 2021.
[19] B. Gholipour, A. Karvounis, J. Yin, C. Soci, and N. I. Zheludev, "Phase-change-driven dielectric-plasmonic transitions in chalcogenide metasurfaces," *NPG Asia Mater.*, vol. 10, no. 6, 2018.
[20] Y. G. Chen, T. S. Kao, B. Ng, et al., "Hybrid phase-change plasmonic crystals for active tuning of lattice resonances," *Opt. Express*, vol. 21, no. 11, pp. 13691–13698, 2013.
[21] P. Hosseini, C. D. Wright, and H. Bhaskaran, "An optoelectronic framework enabled by low-dimensional phase-change films," *Nature*, vol. 511, no. 7508, pp. 206–211, 2014.
[22] F.-Z. Shu, F.-F. Yu, R.-W. Peng, et al., "Dynamic plasmonic color generation based on phase transition of vanadium dioxide," *Adv. Opt. Mater.*, vol. 6, no. 7, p. 1700939, 2018.
[23] Z. Xu, Q. Li, K. Du, et al., "Spatially resolved dynamically reconfigurable multilevel control of thermal emission," *Laser Photon. Rev.*, vol. 14, no. 1, p. 1900162, 2020.
[24] X. Duan and N. Liu, "Magnesium for dynamic nanoplasmonics," *Acc. Chem. Res.*, vol. 52, no. 7, pp. 1979–1989, 2019.
[25] J. Li, Y. Chen, Y. Hu, H. Duan, and N. Liu, "Magnesium-based metasurfaces for dual-function switching between dynamic holography and dynamic color display," *ACS Nano*, vol. 14, no. 7, pp. 7892–7898, 2020.
[26] J. Zidek, A. Milchev, and J. Jancar, "Dynamic responsive formation of nanostructured fibers in a hydrogel network: a molecular dynamics study," *Front. Chem.*, vol. 8, no. 120, p. 120, 2020.
[27] F. Fu, Z. Chen, Z. Zhao, et al., "Bio-inspired self-healing structural color hydrogel," *Proc. Natl. Acad. Sci. Unit. States Am.*, vol. 114, no. 23, pp. 5900–5905, 2017.
[28] F. Fu, L. Shang, Z. Chen, Y. Yu, and Y. Zhao, "Bioinspired living structural color hydrogels," *Sci. Rob.*, vol. 3, no. 16, p. eaar8580, 2018.
[29] J. Jang, K. Kang, N. Raeis-Hosseini, et al., "Self-powered humidity sensor using chitosan-based plasmonic metal–hydrogel–metal filters," *Adv. Opt. Mater.*, vol. 8, no. 9, p. 1901932, 2020.
[30] Y. Wang, Y. Yu, J. Guo, Z. Zhang, X. Zhang, and Y. Zhao, "Bio-inspired stretchable, adhesive, and conductive structural color film for visually flexible electronics," *Adv. Funct. Mater.*, vol. 30, no. 32, p. 2000151, 2020.
[31] Y. Dong, E. M. Akinoglu, H. Zhang, F. Maasoumi, J. Zhou, and P. Mulvaney, "An optically responsive soft etalon based on ultrathin cellulose hydrogels," *Adv. Funct. Mater.*, vol. 29, no. 40, p. 1904290, 2019.
[32] D. Chen, T. Wang, G. Song, et al., "Dynamic tunable color display based on metal–insulator–metal resonator with polymer brush insulator layer as signal transducer," *ACS Appl. Mater. Interfaces*, vol. 11, no. 44, pp. 41668–41675, 2019.
[33] E. Kabouraki, V. Melissinaki, A. Yadav, et al., "High laser induced damage threshold photoresists for nano-imprint and 3D multi-photon lithography," *Nanophotonics*, p 20210263, 2021. https://doi.org/10.1515/nanoph-2021-0263.
[34] C. Liu, Z. Fan, Y. Tan, F. Fan, and H. Xu, "Tunable structural color patterns based on the visible-light-responsive dynamic diselenide metathesis," *Adv. Mater.*, vol. 32, no. 12, p. 1907569, 2020.
[35] Q. Ge, Z. Chen, J. Cheng, et al., "3D printing of highly stretchable hydrogel with diverse UV curable polymers," *Sci. Adv.*, vol. 7, no. 2, p. eaba4261, 2021.
[36] W. Zhang, H. Wang, H. Wang, et al., "Structural multi-colour invisible inks with submicron 4D printing of shape memory polymers," *Nat. Commun.*, vol. 12, no. 1, p. 112, 2021.
[37] Y. Chen, Z. Shu, S. Zhang, et al., "Sub-10 nm fabrication: methods and applications," *Int. J. Extreme Manuf.*, vol. 3, no. 3, p. 032002, 2021.
[38] J. Zhang, C. Huang, Y. Chen, et al., "Polyvinyl alcohol: a high-resolution hydrogel resist for humidity-sensitive micro-/nanostructure," *Nanotechnology*, vol. 31, no. 42, p. 425303, 2020.
[39] R. J. Mancini, S. J. Paluck, E. Bat, and H. D. Maynard, "Encapsulated hydrogels by E-beam lithography and their use in enzyme cascade reactions," *Langmuir*, vol. 32, no. 16, pp. 4043–4051, 2016.
[40] M. W. Knight, N. S. King, L. Liu, H. O. Everitt, P. Nordlander, and N. J. Halas, "Aluminum for plasmonics," *ACS Nano*, vol. 8, no. 1, pp. 834–840, 2014.
[41] R. K. Dey and B. Cui, "Effect of molecular weight distribution on e-beam exposure properties of polystyrene," *Nanotechnology*, vol. 24, no. 24, p. 245302, 2013.
[42] S. Ma, C. Con, M. Yavuz, and B. Cui, "Polystyrene negative resist for high-resolution electron beam lithography," *Nanoscale Res. Lett.*, vol. 6, no. 1, p. 446, 2011.
[43] R. Bonam, P. Verhagen, A. Munder, and J. Hartley, "Performance characterization of negative resists for sub-10-nm electron beam lithography," *J. Vac. Sci. Technol, B*, vol. 28, no. 6, pp. C6C34–C36C40, 2010.
[44] Z. Yang, Y. Zhou, Y. Chen, et al., "Reflective color filters and monolithic color printing based on asymmetric fabry–perot cavities using nickel as a broadband Absorber," *Adv. Opt. Mater.*, vol. 4, no. 8, pp. 1196–1202, 2016.
[45] M. A. Kats and F. Capasso, "Optical absorbers based on strong interference in ultra-thin films," *Laser Photon. Rev.*, vol. 10, no. 5, pp. 735–749, 2016.
[46] N. Ismail, C. C. Kores, D. Geskus, and M. Pollnau, "Fabry–Perot resonator: spectral line shapes, generic and related Airy distributions, linewidths, finesses, and performance at low or frequency-dependent reflectivity," *Opt. Express*, vol. 24, no. 15, pp. 16366–16389, 2016.
[47] L. P. Wang, B. J. Lee, X. J. Wang, and Z. M. Zhang, "Spatial and temporal coherence of thermal radiation in asymmetric Fabry–Perot resonance cavities," *Int. J. Heat Mass Tran.*, vol. 52, no. 13, pp. 3024–3031, 2009.
[48] D. E. Palik, *Handbook of Optical Constants of Solids*, New York, Academic Press, 1985.

Supplementary Material: The online version of this article offers supplementary material (https://doi.org/10.1515/nanoph-2021-0413).